Engineering Science and Technology, an International Journal 58 (2024) 101844

Contents lists available at ScienceDirect

Engineering Science and Technology, an International Journal

journal homepage: www.elsevier.com/locate/jestch

Novel calibration method for improved UWB sensor distance measurement in the context of application for 3D analysis of human movement

Vinish Yogesh [a,b,*], Lisanne Grevinga [a], Carsten Voort [c], Jaap H. Buurke [a,b], Peter H. Veltink [b], Chris T.M. Baten [a,b]

[a] Roessingh Research and Development, Roessinghsbleekweg 33B, 7522 AH Enschede, the Netherlands
[b] Department of Biomedical Signals and System, University of Twente, Drienerlolaan 5, 7522 NB Enschede, the Netherlands
[c] Gable Systems, Granaatstraat 21, 7554 TN Hengelo, the Netherlands

ARTICLE INFO

Keywords:
Ultra-wideband
Distance-bias calibration
UWB calibration
Integrated UWB and MIMU
Distance estimation
Position estimation

ABSTRACT

Integrated UWB and MIMU sensor systems have become popular for pedestrian tracking and indoor localization, since this facilitates data fusion that improves position estimation accuracy by exploiting the complementary nature of their error sources. Integrated UWB/MIMU sensors also have great potential in only on-body use for 3D analysis of human movement, as with MIMU sensors alone accurate direct estimation of (relative) body segment position is not possible. For this, a position estimation accuracy with errors smaller than 1 cm is deemed required. The lowest position estimating error with integrated UWB/MIMU systems, reported so far, is around 5 cm. The main accuracy limiting factors were found to be the systematic errors in the distance estimates from the UWB sensor. Multiple reported attempts to calibrate for these systematic errors failed to achieve the desired accuracy. This article presents a novel distance-bias calibration method that minimizes the residual systematic distance estimate errors using multiple sensors in a swarm configuration. Validation was performed against synthetic reference data and against reference data measured with an optical motion tracking system. Significantly reduced systematic distance estimate errors ($\leq$0.5 cm) were found. These results promise to facilitate significantly better position estimates in future UWB/MIMU data fusion.

1. Introduction

In modern ambulatory 3D analysis of human movement, Magnetic Inertial Measurement Units (MIMUs) have gained popularity due to their low cost, ease of use, and portability [1,2] MIMUs typically provide 3D orientation data in an (inertial) world frame with consistently high accuracy. This is achieved by exploiting redundancy in measured 3D kinematics, including 3D angular velocity, linear acceleration and, often, earth magnetic field data from respectively the three axial rate gyroscopes, linear accelerometers and magnetometers. This is typically done through applying data fusion methods [2–5]. Also, in limited use cases 3D sensor displacement (changes in sensor position over time) is often estimated from the recorded 3D linear acceleration combined with the already estimated 3D orientation [4]. With the starting position known, the 3D position can be estimated in an inertial world frame. However, the accuracy of the 3D displacement estimates, and thus also of the 3D position estimates, is relatively low. They typically suffer from strong estimation drift errors, as double integration of acceleration data is required [6,7]. The integration typically produces high errors as its input signal is already contaminated with accumulated additional errors from the preceding data preparation process on top of the existing inaccuracies in the acceleration signal itself. This makes the application of this approach 'as is' not feasible for relative on-body position estimation, except for short measurements.

Various studies have proposed multiple alternative methods for improved estimation of relative position in the 3D analysis of human movement. These were usually utilizing assumptions on aspects of the movement performed by the human. This involves e.g. applying an extra optimization with constraints to the joint kinematics derived from biomechanical models devised for human movement [8]. This requires biomechanical model constraints that sufficiently fit the subject evaluated and also requires enough excitation (subject movement) for optimization convergence. It is not trivial that this is sufficiently fulfilled in e.g. people with movement disorders. Another example is the Zero-Velocity-Update (ZUPT) algorithm, which detects instances of the foot in stance closest to zero velocity (and foot-flat pose) and restarts the

* Corresponding author.
E-mail address: v.yogesh@utwente.nl (V. Yogesh).

https://doi.org/10.1016/j.jestch.2024.101844
Received 8 May 2024; Received in revised form 13 August 2024; Accepted 19 September 2024
Available online 28 September 2024

integration process delivering 3D displacement, effectively resetting the integration drift to zero, often combined with first-order integration drift removal for the preceding step [9,10]. However, these methods are limited to walking in specific subjects and situations in which this foot placement aspect of walking is taking place sufficiently consistent and detectable, which is specifically questionable in patients. Also, the ZUPT method cannot be used to minimize integration drift in position estimation of sensors on any other body parts than the feet.

An alternate approach to these methods is adding an additional sensing modality to the MIMU sensor hardware, that directly provides time-invariant position or distance estimates. Sensing modalities that were proposed to improve the positional estimates, and were already tested in integration with MIMUs, are distance estimation using miniature Ultrasound (US) [11] and infrared (IR) [12] technology. However, the contribution to the analysis of human movement applications of US is limited due to interference problems when more US tags are used simultaneously [13,14]. The possible application of IR is limited by the strict requirement of direct Line of Sight (LOS) conditions [13]. Other sensor modalities that were proposed to provide position or distance estimates are Wi-Fi, ZigBee, Bluetooth, Radio Frequency Identification (RFID) and Ultra-wideband (UWB) [15–20]. Among these, UWB is reported to be the most accurate with errors lower than 10 cm [21,22].

Therefore, the integrated UWB and MIMU sensors have become popular and have been utilized by many authors for position estimation applications in the last decade [23]. However, to the knowledge of the authors, no articles have been published that utilize this for estimating body segment kinematics in ambulatory 3D analysis of human movement applications with only on-body sensors. Instead, only applications of pedestrian navigation and indoor subject localization applications were reported [23]. For successful application in the 3D analysis of human movement, the technical accuracy of an integrated UWB/MIMU method (UMIMU method) should be similar or close to that of vision-based systems, which are regarded to be the current ‘gold standard’ in clinical movement analysis [24,25]. This suggests that the accuracies of the integrated UWB/MIMU system should have a position estimation accuracy of < 1 cm [26,27].

Current accuracies reported for integrated or combined UWB/MIMU sensor approaches are still far from the desired accuracy for application in 3D analysis of human movement [23]. A majority of the articles reported errors greater than 10 cm and also as high as 1 m, even for optimal Line of Sight (LOS) conditions. The purpose of adding the UWB modality to the MIMU is to stabilize integration drift in displacement/position estimation, by offering time invariant distance/or (relative) position updates to a data fusion-based estimator. Therefore, the quality with which the UWB system can deliver these updates has a great influence on the possible accuracy that can be achieved by the data fusion-based position estimator. Most studies integrating MIMU and UWB sensing have used UWB sensors from one particular market-leading manufacturer (DMW1000 from Qorvo Inc, Greensboro, USA) ‘as is’ and none of them mentioned performing any quality improving or testing calibration procedures [23]. Also, none of these articles mentioned applying the antenna delay calibration that is recommended by the manufacturer. Still, almost all articles report errors that are systematic and that are much larger than what the producing company claims to be achievable (“±5 cm distance error with 99 % probability”). This clearly indicates the presence of systematic errors much larger than what is required for application in 3D analysis of human movement in the UWB distance estimates, an observation that was also confirmed in other studies [28,29].

Multiple attempts to develop methods for calibration or correction of systematic errors in UWB distance estimates were reported in literature [28–33]. All these studies except [28] targeted specific aspects of UWB internal parameters e.g. the error introduced due to the skewness between the clocks of ranging UWB sensor nodes [29,31,33], and antenna delays [30,32]. One study estimated distance errors between each sensor combination from the received signal strength (RSS) and only tested this at the exact same location [28]. As RSS strongly depends on environmental factor details, this paper generated strong doubts about generalizability. Among all the other calibration methods, the lowest systematic error reported to have been achieved after the calibration was around 3 cm [31]. Also, in initial (own) pilot studies the authors of this paper found persistent residual errors greater than 4 cm in structural ranging components, even after performing the recommended antenna delay calibration by Qorvo [32].

Summarizing all results reported, the presence of persistent substantial systematic errors is the main factor preventing a position estimation accuracy through UWB/MIMU data fusion that is required for 3D analysis of human movement. This article proposes a generalizable one-time calibration method for reducing the systematic UWB distance estimate errors to sub-centimeters and validates its performance against the gold standard method within the distance value range relevant to 3D analysis of human movement. As such, the article examines whether this method could facilitate the future development of MIMU/UWB data fusion methods for this application. The method utilizes data from a swarm of UWB sensor nodes. It applies an optimization procedure that exploits the redundancy in a set of UWB node distance estimates recorded during a ‘random’ movement within the relevant distance range. For this, it uses a simple distance bias error model. In this article, this method is referred to as the ‘distance-bias calibration method’.

2. Methods

2.1. UWB ranging method and configuration

The UWB sensors used in this research estimate distances between sensor nodes based on the Time of Flight (ToF) information, which is also the most popular and commonly used technique for distance measurement using these sensors [34]. The distances were estimated using the available information on ToF and the known speed of the UWB transmission. For the ToF estimation, the method/algorithm implemented was the Alternative Double Sided-TWR (AltDS-TWR) [35]. The AltDS-TWR method is the most robust and popular approach used to deal with the internal clock drift between unsynchronized UWB nodes in ToF measurements [36]. This AltDS-TWR is also the current state-of-the-art approach used in most of the commercial UWB sensors such as the DW1000. In addition, the antenna delay calibration was applied, as recommended by Qorvo [32], for all the UWB sensor nodes that were used for this research.

Since the targeted use case application in this research is full body 3D analysis of human movement, a swarm topology is used for the UWB ranging, as opposed to the star topology typically used in tracking applications. The swarm topology uses a fully connected network that performs the UWB distance-ranging operation between all pairs of UWB sensor nodes present in the network. This typically delivers redundant data for estimating node relative positions applying e.g. an optimization approach. This swarm topology implementation is illustrated in Fig. 1. In this implementation, one additional sensor node, not participating in the ranging, assumed the role of a controller and listener (green node in Fig. 1). This ‘controller node’ was connected to a PC with a user interface for configuring and operating the sensor system. This node controlled the overall timing of the ranging protocol and relayed any operational command to the ranging sensors. It also acted as a listener device and collected all distance estimates from all nodes in the network along with the MIMU data and uploaded this data to a PC via USB for processing. This swarm configuration yields (n-1)! distance estimates for a set of n UWB sensor nodes per update in a fully connected swarm of n sensors.

2.2. Proposed distance-bias calibration

2.2.1. Error model

The distance-bias calibration error estimation model in this research was built for multiple swarms of three UWB sensor nodes (the minimum

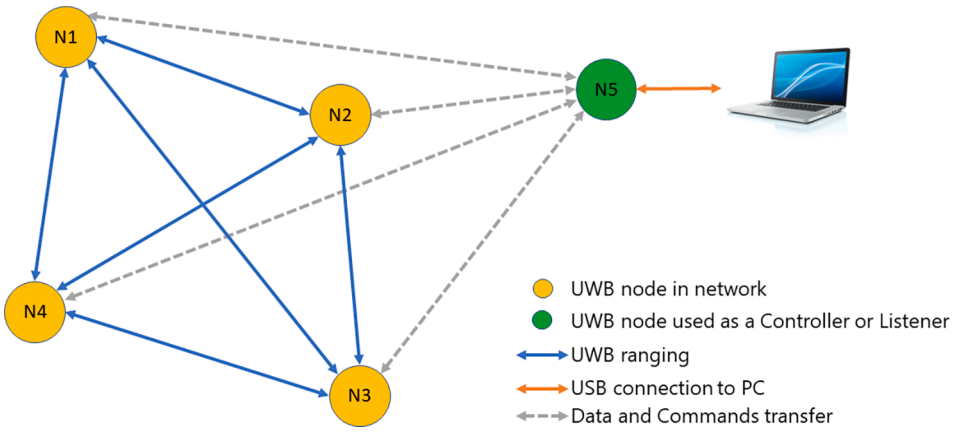

Fig. 1. Configuration and swarm topology of identical UWB nodes. The nodes taking part in the ranging process (yellow) switch roles between the ranging initiator and ranging responder following a fixed round-robin scheme installed in all of them by the controller/listener node (green).

required to form a swarm), also for reasons of optimizing computational load (Fig. 2). The UWB sensor nodes participating in the ranging are identified as 'Node i' where i corresponds to the sensor number with $i \in N$. A priori unknown position within the sensor node casings between which the distance was actually measured was named the UWB center point, C_i (blue dots in figure). UWB center points, C_i were assumed to be on or close to the antenna of the UWB unit inside the sensor casing. The distances measured between the C_i points in a pair of sensor nodes i and j were defined as $D_{uwb\ i,j}$ and the distance between the sensors $D_{i,j}$ is indicated with blue lines in the figure. A physical reference point on the sensor casing that can be measured using any external reference system is defined as the UWB casing frame origin, P_i . The position of P_i with respect to the global reference frame was represented as $\overrightarrow{P_i}$ (yellow vectors). The position of UWB center point, C_i with respect to the UWB casing frame origin, P_i was represented as UWB center point vector, $\overrightarrow{C_{g,i}}$ in the global frame. Since all the UWB nodes were physically identical in hardware and ran the same embedded software, it was assumed that all the vectors $\overrightarrow{C_{g,i}}$ (orange vectors) are identical for all the sensor nodes in the sensor frame and will be always represented as $\overrightarrow{C_s}$. The position of UWB center point C_i relative to the origin of the global reference frame is indicated by $\overrightarrow{K_{g,i}}$ (green vectors).

The error model was built based on the assumption that both the UWB nodes participating in a ranging operation contribute individually to the bias error in the distance estimated with a fixed contribution. It is assumed that the main errors in determining the ToF and distance are formed by systematic, but unknown, time delays, that are caused by delays inside sensor hardware and software and which therefore are not related to the distance between the sensors. All these probable error causes are assumed to occur to the same extent in each ranging operation. Besides this, these errors can be generalized as a single error corresponding to each sensor irrespective of the source of error being attributed to transmission and reception errors, since the AltDS-TWR ranging protocol ensures that both operations occur twice in each sensor. Consequentially they are modeled as sensor-specific bias errors. Earlier studies into ranging errors within the relevance of human tracking did not report an effect of the distance between the ranging UWB nodes on the reported distance estimation [23]. This suggests that the observed non-random estimation error components were mainly pure bias errors and did not contain gain effects. This was again confirmed by an initial extensive error evaluation of all pairs of two UWB sensor nodes within the distances relevant for 3D analysis of human movement. Therefore, in this study estimation errors were modeled as pure bias errors. This allowed for the distance estimation bias errors to be modeled as the sum of the two bias error contributions eb_i and eb_j of both involved UWB sensor nodes i and j. Then the estimated

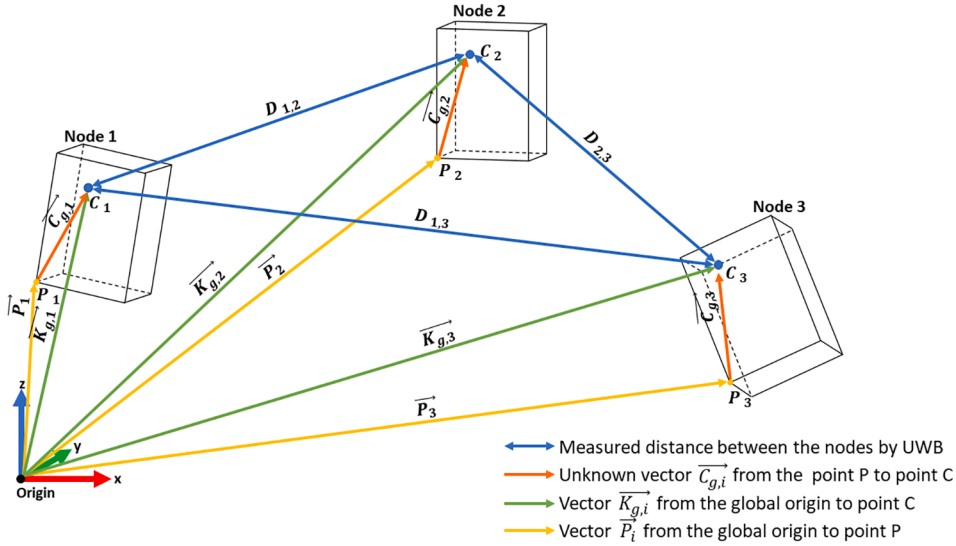

Fig. 2. Illustration of the swarm measurement model. Note that the externally observable distances P_i (e.g. by a reference system) are different from the measured distances C_i in any situation except the situation in which the 3D orientation of all sensor nodes is exactly equal.

distance between them, $D_{uwb\ i,j}$, can be written as

$$D_{uwb\ i,j} = D_{true\ i,j} + eb_i + eb_j \quad (1)$$

Here, $D_{true\ i,j}$ is the true distance between the two UWB Center points C_i and C_j. Considering the ranging operation between two UWB sensor nodes i and j in a swarm of n sensor nodes, the true distances between the nodes i and j, $D_{true\ i,j}$ can be also defined in terms of the global coordinate vector to the UWB center point, $\overrightarrow{K_g}$ and is given as

$$D_{true\ i,j} = \left|\overrightarrow{K_{g,i}} - \overrightarrow{K_{g,j}}\right| \text{ for } i,j \in [1,n] \quad (2)$$

combining equations (1) and (2), and defining them in terms of the true distance $D_{true\ i,j}$ gives

$$D_{true\ i,j} = \left|\overrightarrow{K_{g,i}} - \overrightarrow{K_{g,j}}\right| = D_{uwb\ i,j} - eb_i - eb_j \text{ for } i < j \quad (3)$$

The position of C_i relative to the origin of the global reference frame, $\overrightarrow{K_{g,i}}$ can be derived based on the geometric relations as seen in Fig. 2 through vector addition. With this considered, the following relation can be derived for the global coordinate vector to the UWB center point, $\overrightarrow{K_g}$ from the UWB casing frame origin, P_i and center point vector, $\overrightarrow{C_{g,i}}$:

$$\overrightarrow{K_{g,i}} = \overrightarrow{C_{g,i}} + \overrightarrow{P_i} \text{ for } i \in [1,n] \quad (4)$$

As previously mentioned, all the vectors $\overrightarrow{C_{g,i}}$ were assumed identical for all the sensor nodes in the sensor frame. This implies that the vectors $\overrightarrow{C_{g,i}}$ are the vector in the sensor frame, $\overrightarrow{C_s}$ rotated to the global frame. Therefore, with a known orientation of the sensor node the $\overrightarrow{C_{g,i}}$ can be estimated as:

$$\overrightarrow{C_{g,i}} = q_i^* \overrightarrow{C_s} q_i \text{ for } i \in [1,n] \quad (5)$$

Where q_i is the orientation of sensor node i expressed as unit quaternion in the global reference frame, while q_i^* is the conjugate of the quaternion q_i. Substituting equation (5) in 4:

$$\overrightarrow{K_{g,i}} = q_i^* \overrightarrow{C_s} q_i + \overrightarrow{P_i} \text{ for } i \in [1,n] \quad (6)$$

Substituting equation (6) in 3 provides the final model which then can be used to estimate the unknown parameters eb_i and $\overrightarrow{C_s}$ by optimization. Thus, the model is defined as:

$$\left\| \left(q_i^* \overrightarrow{C_s} q_i + \overrightarrow{P_i}\right) - \left(q_j^* \overrightarrow{C_s} q_j + \overrightarrow{P_j}\right) \right\| = D_{uwb\ i,j} - eb_i - eb_j \quad (7)$$

In this equation the measured distance between each node $D_{uwb\ i,j}$, the position of the node casing $\overrightarrow{P_i}$ and the node orientations q_i are the known variables that were measured. The UWB center point vector, $\overrightarrow{C_s}$ and the bias errors eb_i and eb_j are the unknown variables. When expanding these equations to a form suitable for numerical evaluation, some of the unknown variables appear in quadratic terms. This means that evaluation requires a non-linear optimization method.

For three UWB nodes, this expansion yields 3 equations with 6 unknowns. For n nodes, this yields n-1 triangular number of equations:

$$no.ofequations = 1 + 2 + \cdots + (n-1) \text{ for } n \in N \quad (8)$$

Also, this yields a total of n + 3 unknowns. This makes this set of equations an underdetermined ($n < 5$) or overdetermined ($n \geq 5$) system suggesting the application of an optimization approach to a set of multiple samples at different distance combinations to solve for the unknown bias errors eb_i and UWB center point vector, $\overrightarrow{C_s}$.

2.2.2. Optimization approach

A multi-objective constrained non-linear optimization method was applied to estimate the unknown bias errors eb_i and $\overrightarrow{C_s}$ by minimizing the differences between D_{true} and $D_{uwb} - eb_i - eb_j$, utilizing the model defined in equation (7).

$$Min\left(\left\| \left(q_i^* \overrightarrow{C_s} q_i + \overrightarrow{P_i}\right) - \left(q_j^* \overrightarrow{C_s} q_j + \overrightarrow{P_j}\right) \right\| - \left(D_{uwb\ i,j} - eb_i - eb_j\right)\right) \text{ for } i,j \in N \quad (9)$$

This was done by applying the non-linear optimization method of Nelder-Mead (NMinimize function implemented in Wolfram Mathematica version 12.1). Two constraints are included to improve the chances and speed/computational load of convergence to the global best solution. The first constraint limits the solution space of the UWB center point, C_i to a volume derived from the UMIMU sensor's physical dimensions assuming that C_i is on, or very near, the antenna surface and inside the sensor casing. As a consequence, $\overrightarrow{C_s}$ was limited to positive values with maximum coordinate values chosen equal to the dimensions of the sensor node casing. The second constraint limits the bias error estimates to be always positive, which were based on reasoning confirmed in all pilot test results, that the ranging errors are caused by an apparent overestimation of ToF values. The bias error upper limits were constrained to a worst-case maximum of 15 cm, also based on results of pilot experiments yielding distance estimate errors never greater than 15 cm.

2.3. Validation with synthetic data

Synthetically generated distance estimates with predefined bias error values eb_i and UWB center point values C_i were used for directly validating the performance of the calibration algorithm. Additionally, to evaluate the convergence of the optimization requires the synthetic data in which the true values of eb_i and C_i are known as opposed to them not being known in experimental data. The data were generated with a custom-built data generator, mimicking a physically realistic movement (speed of movement and change in orientations limited to a normal human movement scenario) for a set of three sensors named S1, S2 and S3 respectively. The resulting distances between all three sensor pairs were provided as an output of the data generator, with the distance combinations between the sensors being labeled with their number assigned to them (For example: the distance between S1 and S2 sensors was labeled as $D_{uwb\ 1,2}$). The distance update rate of the generated data was set to 10 samples per second, which was close to the general update rate of commercial UWB sensors. To achieve realistic translation and rotation of the sensor's data for each timestep, these were randomly drawn from a uniform distribution with a minimum of 1 degree and maximum of 5 degrees for the change in rotation of the sensor and with a minimum of 5 cm and a maximum of 20 cm for the change in sensor position. In addition to this, white noise with an SD of 2.5 cm was added to the generated distance data. Noise SD values were based on the experimental evaluation of UWB ranging. A total of 30 data sets were generated with varying values for $\overrightarrow{C_s}$ and eb_i randomly drawn from uniform distributions ($0 < C_x < 5$, $0 < C_y < 4$, $0 < C_z < 0.8$, $-15 < eb_n < 15$) and the resulting sensor distances were fed as inputs into the optimization algorithm. For each of the 30 generated data sets, the optimization procedure was repeated 30 times, each time with a different random permutation of the input data and different initial vector values randomly drawn from uniform distribution within the given constraints. The estimated values of $\overrightarrow{C_s}$ and eb_i with the lowest residual error in a set of 30 optimizations were considered as the final estimates. The resulting parameter estimates for $\overrightarrow{C_s}$ and eb_i were compared against the ground truth values used in the synthetic data generation. Additionally, the errors of the calibrated distances were compared against the distance errors before the calibration of the distance estimates.

2.4. Validation with experimental data

2.4.1. UWB sensor hardware and calibration setup

A custom fully integrated UWB/MIMU sensor hardware platform

was developed in-house, the sensors of which were named 'UMIMU' sensors (Ultra-wideband Magnetic Inertial Measurement Unit sensors) and were used in this research. UMIMU sensors consist of a UWB transceiver module DW1000, a 9-axis MTi-3 MIMU (Xsens Technologies, Enschede, Netherlands), an STM32F722RE microcontroller (STMicroelectronics, Geneva, Switzerland), USB communication for charging, configuration and programming combined on a custom PCB (Fig. 3a). The UWB sensor nodes estimate the distance between them by the AltDS-TWR method as described in Section 2.1. The onboard MIMU is sampling independently using the MIMU chip clock at 100 samples per second to deliver 3D orientation, acceleration and angular velocity. The UWB onboard the UMIMU sensor platform is controlled by the clock of the microcontroller of the sensor platform. The UWB update rate depends on the number of rangings requested within one update and was recorded at an update rate of 15 samples per second (with 4 UMIMUs in a fully connected swarm). Each UWB update is attributed to the same time instant as the last MIMU update. This yields a synchronization uncertainty of $\pm$ 0.0099 s between the UWB data and the MIMU data. This paper only utilizes the UWB sensors in the UMIMU modules, while the MIMUs on-board are only used for synchronization between the UWB and camera-based motion analysis system.

For the purpose of validation and for obtaining data necessary for the calibration algorithm such as $\overrightarrow{P_i}$ and q_i, a camera-based motion analysis system Vicon (Vicon Motion Systems Ltd, Oxford, UK) was used due to its capability of sub-centimeter level accuracy for marker position estimation. A special sensor-holding rig with reflective markers (Fig. 3b) was designed to aid the estimation of the necessary parameters. The rig had three reflective markers (labeled M1 to M3) mounted on sticks (Fig. 3b and 3c). A local right-handed reference frame was derived for each rig from the three markers. The UWB casing frame origin, P_i was defined as being located at the right-bottom corner of the sensor PCB (yellow dot, Fig. 3a). The casing reference frame X-axis and Y-axis were defined parallel to the ribs of the PCB and the Z-axis was defined perpendicular to the rig base plate. For consistent estimation of the sensor orientation q_i and position P_i, the sensors are always aligned to the two sides of the rig base as seen in Fig. 3c. This is followed by an initial rig calibration procedure performed before the start of the distance-bias calibration protocol. The rig calibration procedure was a static measurement of the rig markers along with the UMIMU sensor mounted with an additional temporary marker placed on the position P_i. This static measurement was used for deriving the relation (translation and rotation) between the rig reference frame and the sensor frame. This then would be applied for the calibration measurement with the marker on P_i removed to avoid possible interference of the marker on P_i with the UWB antenna function. The orientation of the sensor rig q_i was defined as the orientation of this local rig reference frame with respect to the global reference frame (defined by the global Vicon system reference frame).

2.4.2. Calibration experiment/protocol

The distance-bias calibration algorithm requires an input dataset that consists of a wide range of sensor distances and different sensor orientations to facilitate the convergence of the optimization process across different scenarios and conditions. Therefore, in each calibration session, a series of sensor node movements were chosen to contain sufficient variations in node distances and orientations in a volume of interest for the intended application of analysis of human movement.

The experimental validation was performed with the UMIMU sensor system, and a reference optical motion capture system as described in Section 2.4.1. The calibration was performed by two persons moving two wooden sticks, with a sensor-holding rig with a sensor attached to the end of each stick (Fig. 4, right). Maximal care was taken to prevent any interference or NLOS situation through the bodies of the 2 persons performing the calibration protocol. Two sets of 4 sensors were used for the experimental validation, and they were named Set-A (sensors 1, 2, 3 and 4) and Set-B (6,7, 8 and 9). Sensor 5 was assigned to be the controller/listener for both sets.

Two calibration movement protocols, differing in the movements made were performed to test the optimization performance. In protocol 1, two persons held a calibration stick with a rig and sensor in each hand, while facing each other, (Fig. 4-left) and made random free-arm movements while the persons remained in the same position for the duration of the protocol. In protocol 2 the two persons start in the same position and pose again facing each other while making random free-arm movements. In addition, they moved slowly in circles of about 1.5 m in diameter, while keeping the same distance, facing each other and keeping the sticks in between them, again maximally avoiding any NLOS situation. Both protocols were performed for both set A and set B. All measurements lasted approximately 3 min and were repeated twice, yielding 'trial 1′ and 'trial 2′ for each protocol.

For each protocol, only the first 800 samples of the data from trial 1 (the 'training set') were fed into the calibration optimization process. Since the optimization algorithm was developed for sets of three sensors, this procedure was repeated for all four possible subsets of both set A and set B. For set 1, the four subsets were named set-123, set-234, set-341 and set-412. Similar naming was given to the subsets of set B. The optimization was then repeated 30 times for each of these combinations. The estimated values of $\overrightarrow{C_s}$ and eb_i with the lowest residual error in a set of 30 optimizations were considered as the final estimates. As the results of all four subsets yielded more than one estimate, the final estimates for the values of eb_i and $\overrightarrow{C_s}$ were computed by averaging the resulting values for eb_i (2 for each sensor) and $\overrightarrow{C_s}$ (4 estimates) respectively.

In the experimental validation, it is not possible to directly compare the estimated distances after calibration against its ground truth values, because the gold standard reference system does not deliver ground truth values for $\overrightarrow{K_{g,i}}$ and therefore not for $D_{i,j}$. Instead, it only delivers

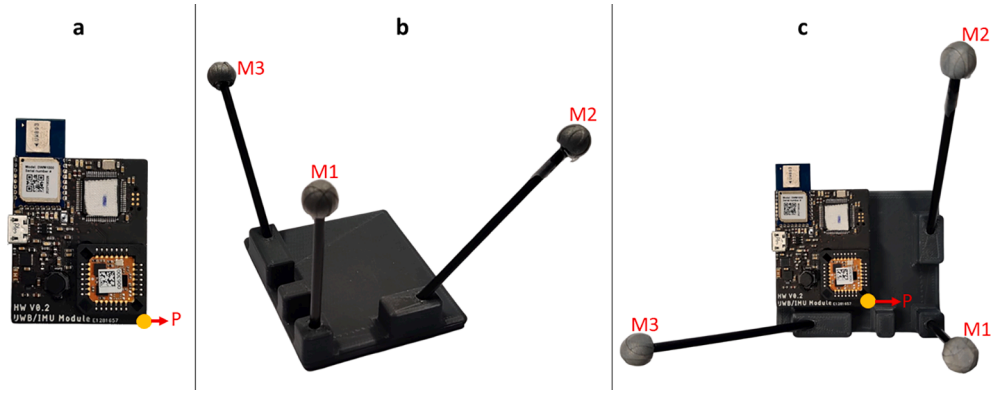

Fig. 3. a) UMIMU sensor module; b) Sensor holding rig with reflective markers; c) Experimental setup with UMIMU sensor fixed to the rig.

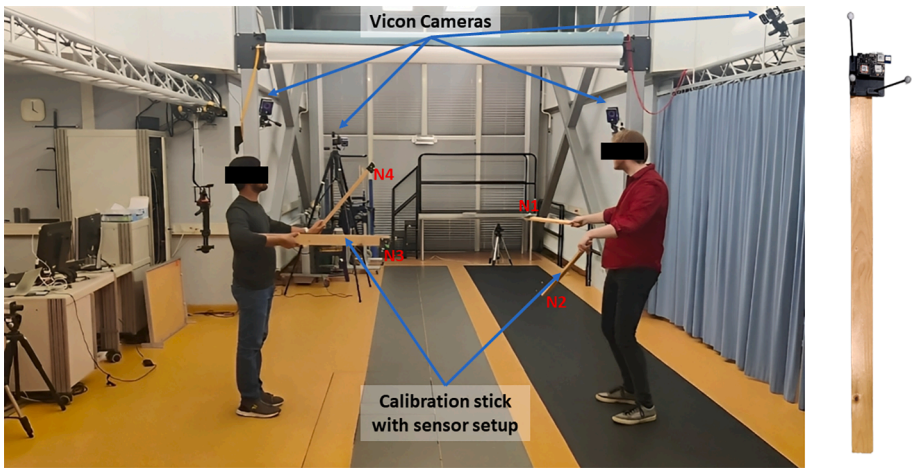

Fig. 4. Calibration protocol situation with four UWB nodes labeled N1 to N4 along with the reference VICON system cameras (left) and the calibration stick with the sensor setup (right).

ground truth values for $\overrightarrow{P_i}$. Therefore, estimated distances after calibration were validated against a virtual ground truth value for $D_{i,j}$, named $D_{ref\,i,j}$, being the distance between the virtual $\overrightarrow{K_{g,i}}$ values that were estimated from known values of $\overrightarrow{P_i}$ and q_i from Vicon and the estimated values $\overrightarrow{C_s}$ from the optimization results. First, validation was performed for the values from the training set. Then a validation was performed for a 'validation set' containing the remaining values of trial 1 and trial 2 for each protocol.

2.4.3. Calibration process pipeline

In the swarm calibration process pipeline (Fig. 5), first the positions of the markers attached to the sensor node rig were estimated through the Vicon system. Secondly, the UMIMU sensor nodes provided the distance estimates, $D_{uwb\,i,j}$ (as well as all 3D orientation, angular velocity and acceleration estimates, for future studies) of each node in the network. The position estimates of the Vicon system were used to obtain the orientation q_i and the vector to the UWB casing point, $\overrightarrow{P_i}$. This information was also used to estimate the distance between the sensor nodes D_{true} which then was later used for estimating the accuracy of the UWB distance estimates D_{uwb}. Synchronization of the UMIMU and Vicon systems was done by lining up the acceleration magnitude estimates of both systems for the same node/rig (applying a cross-correlation approach) measured at 100 samples per second.

2.5. Data analysis

For both validation with simulated synthetic data and with experimental data the accuracy of the swarm calibration method was computed for each condition through estimated confidence intervals and correlation coefficients between UWB-based and ground-truth reference estimates. Additionally for the synthetic data, the accuracy of estimation of the values of $\overrightarrow{C_s}$ and eb_i were computed based on a direct comparison between the values used as input for data generation and the values of $\overrightarrow{C_s}$ and eb_i estimated by the swarm calibration method. Reproducibility and consistency of the distance-bias calibration method were evaluated for both the generated and synthetic data sets through statistical moments of the distributions of the 30 calibration results per set and summarized over all the generated sets.

3. Results

3.1. Validation results with synthetic data

For the synthetic data, the distance estimates after calibration were clearly more accurate than the ones before and very closely followed the ground truth distance measures, as illustrated in a typical example (Fig. 6).

The distance-bias calibration has successfully removed the systematic bias component in the distance estimates, which have significantly reduced from around 35 cm to around −0.4 cm. The mean distance error before the calibration varied widely between the data sets generated, as they were based on the input values of $\overrightarrow{C_s}$ and eb_i (Fig. 7). The mean distance errors before calibration over all the 30 data sets were 35.1 ± 11.1 cm, 35.5 ± 11.0 cm and 36.0 ± 12.3 cm for the ranging sensor pairs 12, 13 and 23 respectively (Fig. 7-Top). The standard deviation (SD) values of these errors before calibration were a direct result of the noise parameters set for the synthetic data generator (Section 2.3) and were around 2.5 cm. The average distance errors after calibration over all the 30 data sets with unique $\overrightarrow{C_s}$ and eb_i values were −0.46 ± 2.58 cm, −0.35 ± 2.60 cm, −0.35 ± 2.53 cm for the ranging sensor pairs 12, 13 and 23 respectively. The SD values of the errors after calibration were

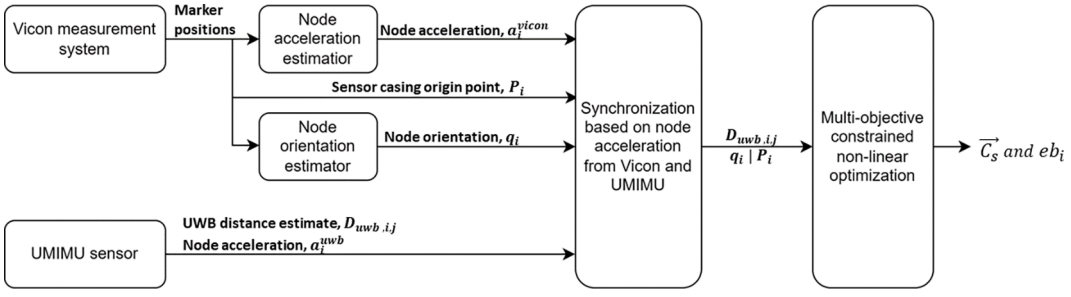

Fig. 5. Schematic of the distance-bias calibration process pipeline.

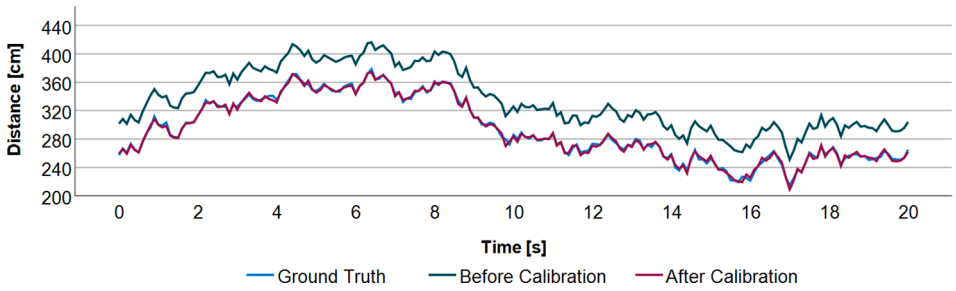

Fig. 6. Typical example of distance estimates before (green) and after calibration (red) along with their reference distance (blue) for the synthetic data set.

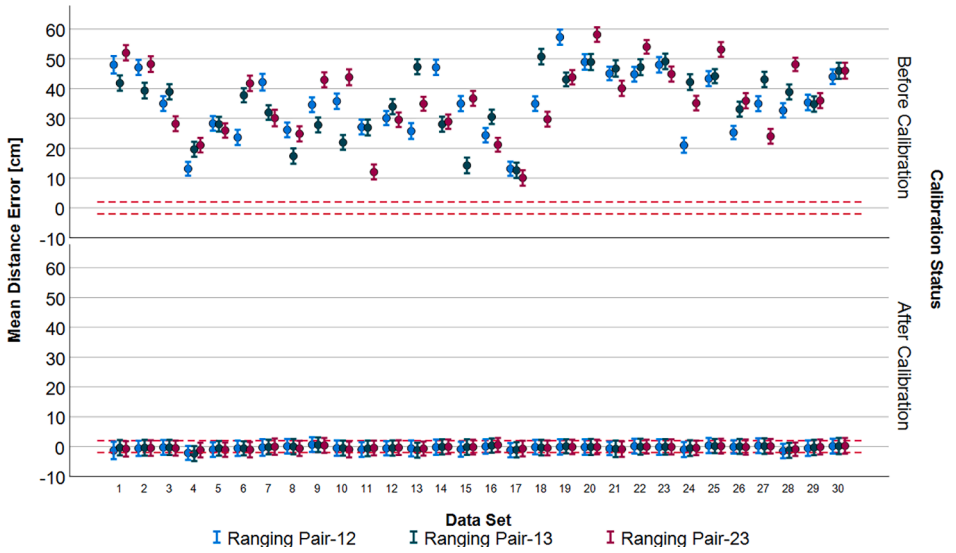

Fig. 7. Mean and standard deviation (whiskers) of distance errors before (top) and after the calibration (bottom) for all the 30 synthetic data sets generated of the three ranging sensor pairs. The dotted red lines are 2 cm away from the graph's origin line on both the positive and negative axes.

again around 2.5 cm (Fig. 7-Bottom).

For all three simulated sensors, the mean absolute errors (MAE) of the estimated bias values eb_i were always less than 1 cm for almost all the 30 different data sets (Fig. 8-Top), with one outlier in synthetic data set-4 (MAE of 1.70 cm for eb_1). For all the 30 data sets, the average of the MAE in bias estimation was 0.33 ± 0.34 cm, 0.31 ± 0.22 cm and 0.30 ± 0.24 cm for eb_1, eb_2 and eb_3 respectively. The MAE of the estimated UWB center point, C_s was always less than 0.75 cm for almost all the 30 different data sets (Fig. 8-bottom), except for one of the three co-ordinates for three data sets (MAE of 1.1 cm for C_x in data set-11; MAE of 1.31 cm and 1.14 cm for C_y in data set-13 and 19 respectively). For all the 30 data sets, the average of the MAE in UWB center point estimation

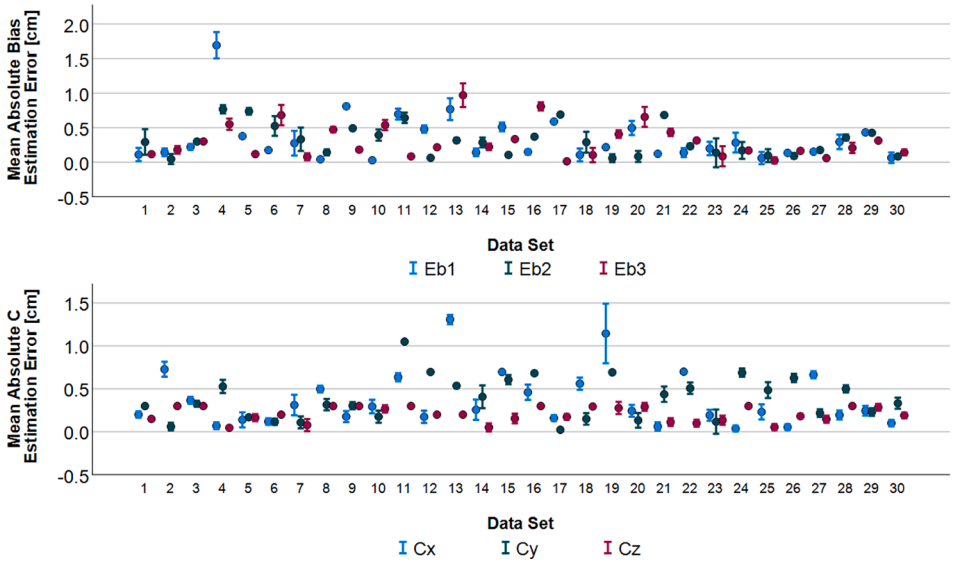

Fig. 8. Bias estimation errors for all three sensors (Top) and the UWB center point estimation errors (Bottom) for the synthetic data set.

was 0.37 ± 0.32 cm, 0.38 ± 0.24 cm and 0.21 ± 0.09 cm for C_x, C_y and C_z respectively.

The repeatability of the optimization is indicated by the residual error of the optimization procedure for iteration within a specific data set and is found to be very consistent over the 30 data sets (Fig. 9). The average error of the mean residual errors over all the data sets was estimated to be 2.2 cm with an SD of 0.1 cm.

3.2. Validation results with experimental data

Similar to the synthetic data set, the distance estimates after the calibration for the experimental data were clearly found to be more accurate than those before and closely followed the ground truth distance values. This is illustrated in a typical example of the distances measured between two nodes in an experiment (Fig. 10).

For the experimental training data set, the distance-bias calibration has removed the systematic bias component in the distance estimates, which have reduced from around 3.7 cm and 2.1 cm to around 0.5 cm and −0.5 cm in protocol 1 and protocol 2 respectively (Fig. 11). The random distance errors before calibration for each of the 12 ranging combinations were around 11.0 cm and 12.0 cm in protocols 1 and 2 respectively. After applying calibration these only improved marginally to 9.7 cm and 10.6 cm in protocol 1 and 2 respectively, though the distance-bias calibration is not intended for dealing with the random errors. The mean distance errors after the calibration for almost all individual ranging combinations improved in both protocols applied, except for a single ranging sensor pair 89 in protocol 2. This specific pair had a higher mean error of −7.3 cm (Fig. 11).

For the experimental validation data set, similar to the previous results distance-bias calibration has removed the systematic bias component in the distance estimates. The systematic errors have reduced from around 2.5 cm and 2.6 cm to around −0.3 cm and −0.5 cm in protocol 1 and protocol 2 respectively (Fig. 12). The random distance errors before calibration for each of the 12 ranging combinations were around 11.4 cm and 11.5 cm in protocol 1 and 2 respectively. After applying calibration these only improved marginally to 10.2 cm and 10.5 cm in protocol 1 and 2 respectively. Similar to the training data set, mean distance errors after the calibration for almost all individual ranging combinations improved in both protocols applied, except for a single ranging sensor pair 89 in protocol 2. This specific pair had a higher mean error of −7.7 cm (Fig. 12). In addition, the mean systematic errors before the calibration for all the sensor ranging combinations when compared against the distance between the $\overrightarrow{P_i}$ (without considering the orientation of the sensor, i.e., estimated $\overrightarrow{C_i}$), were −4.5 cm and 4.6 cm in protocol 1 and 2 respectively. For all the optimization combinations the mean residual error at solution convergence was always around 5 cm. Also, the mean residual value of all the iterations is 5.91 cm with an SD of 2.51 cm.

4. Discussion

Over all tested situations the distance estimates were found to be substantially closer to the true distance values after applying the proposed distance-bias calibration method. For both the validations with synthetic data and experimental data, the estimates for distance $D_{i,j}$ consistently showed a higher accuracy with the distance-bias calibration procedure applied than without (Fig. 6 and Fig. 10). After calibration, systematic estimate errors were consistently around or below 0.5 cm for both validations. The non-linear optimization procedure did consistently converge over multiple repetitions for each condition.

For the synthetic data, the systematic errors of the full procedure reduced significantly from around 35 cm to −0.4 cm, and the distance error magnitude was consistently lower than 2 cm for all the 30 underlying unique data sets used. The accuracy of the distance-bias calibration method in estimating the values of the unknown UWB center point vector, $\overrightarrow{C_s}$ and the ranging bias errors eb_i was only directly validated with the synthetic data set, since it is not possible to assess their true values directly in the experiments. The estimation errors in these parameters were consistently found to be at a sub-centimeter level over all 30 different synthetic data sets (Fig. 8). All validation results for the synthetic data support the conclusion that the distance-bias calibration procedure seems capable of consistently improving distance estimates to the desired level by accurately estimating of $\overrightarrow{C_s}$ and eb_i.

For the experimental data, a very similar consistent improvement of applying the distance-bias calibration was found as for the synthetic data. Distance-bias calibration performed almost equally for both the protocols tested with the residual systematic bias being −0.3 cm and −0.5 cm in protocol 1 and protocol 2 respectively. Although the difference in performance was very small between the two protocols overall performance of protocol 1 is better than the other. This could be due to the nature of movement in protocol 1 where the subjects performing the calibration were standing still and probably had minimal chances of introducing accidental NLOS, which can occur when subjects are moving as in protocol 2. The random component of the distance error (SD) was comparatively larger than the ones found for the synthetic data set. For the experimental data, the estimation accuracy of $\overrightarrow{C_s}$ and eb_i were not validated directly as they cannot be measured with a reference method. However, the estimates for the effective UWB center point C_i position was found to be close to the position of the antenna center position within the casing.

The proposed calibration algorithm delivered very reproducible distance estimation accuracy results as illustrated by consistent SD values of the low residual errors achieved (Fig. 9). For the synthetic data set these were consistently close to each other over 30 permutations within each combination of input parameters $\overrightarrow{C_s}$ and eb_i with SD values always lower than 0.1 cm. Also, the estimates of the unknown parameters $\overrightarrow{C_s}$ and eb_i were consistently close to the true value for all tests with synthetic data. The residual errors for the experimental data also showed good reproducibility (SD 2.5 cm). For the experimental data, the results for distance estimation resembled the ones for the simulated synthetic data set in their consistent strong improvement of accuracy in the estimation of distance $D_{i,j}$. This suggests that for the experimental data, the values for eb_i (as well as $\overrightarrow{C_s}$) were also estimated with similar

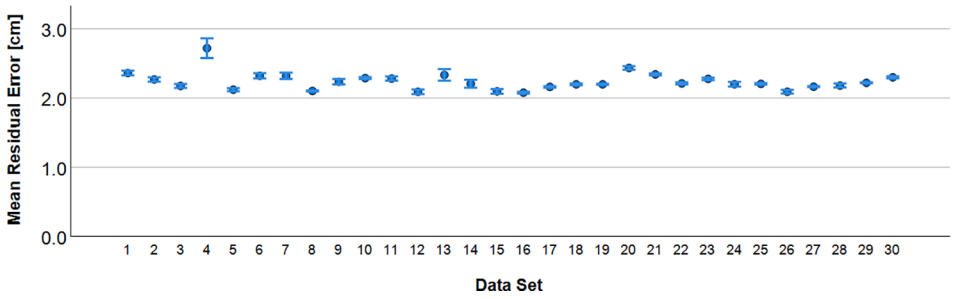

Fig. 9. The residual error of the optimization procedure for all the 30 data sets in the synthetic data set.

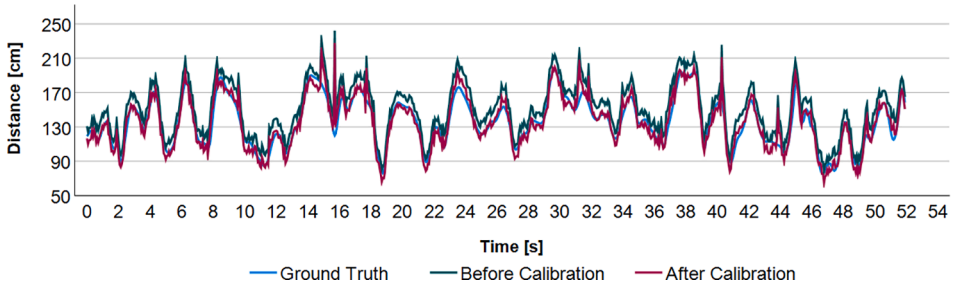

Fig. 10. Typical example of distance estimates from UWB sensors before calibration (green) and after calibration (red) along with their reference distance (blue) from the Vicon optical system concerning the experimental data.

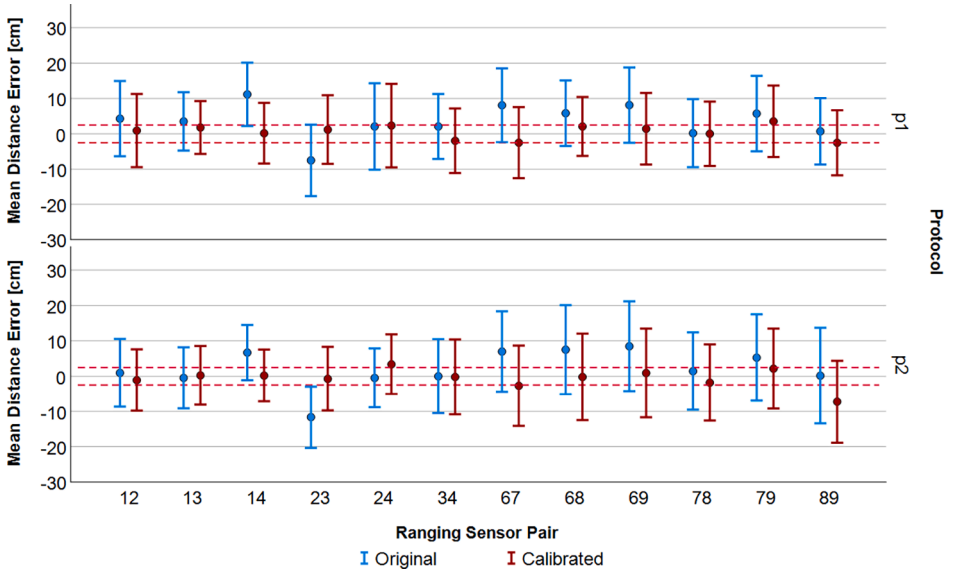

Fig. 11. Mean distance estimation error before (blue) and after (red) distance-bias calibration for each ranging combination for both the protocols validated for the experimental training data set. Dots represent the systematic distance estimation errors, and the whiskers indicate the distance estimation error SD, that is random error component. The dotted red lines are 2.5 cm away from the graph's origin line on both the positive and negative axes.

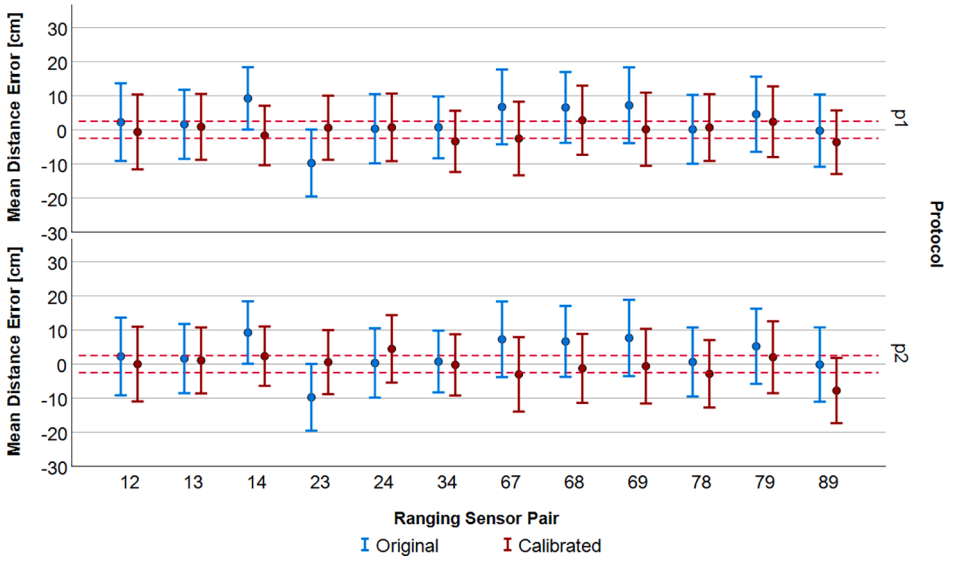

Fig. 12. Mean distance estimation error before (blue) and after (red) distance-bias calibration for each ranging combination for both the protocols validated for the experimental validation data set. Dots represent the systematic distance estimation errors, and the whiskers indicate the distance estimation error SD, that is random error component. The dotted red lines are 2.5 cm away from the graph's origin line on both the positive and negative axes.

accuracy as for the synthetic data.

All other calibration methods proposed in the literature calibrate parameters at the hardware level, in attempts to directly correct for sources of the error [29–33]. They mainly address errors of clock drifts, and antenna delays directly. However, the distance-bias calibration method proposed in this paper is a more phenomenological approach directly addressing the observed errors. Therefore, a direct comparison against these other methods is not possible. Additionally, the proposed calibration was performed with the UWB sensors that were first calibrated at the hardware level (antenna calibration). Residual systematic errors of around 3 cm were present even after the antenna calibration in the distance ranges (Fig. 11 and Fig. 12). Thus, the proposed calibration appears to reduce the systematic errors significantly over all of these other calibration methods at the hardware level [29–33], which report systematic errors of less than 3 cm [31], and around 6 cm [29], 7 cm [30], 5 cm [32] and 29 cm [33] respectively. Though [31] had achieved accuracies closer to our proposed method have only been validated in a controlled static measurement, while the validation in this study is during a more dynamic movement. Also, the smaller systematic errors achieved with the proposed distance-bias method indicate that apparently, none of them tackles all error sources sufficiently.

Additionally, the effect of the orientation differences between UWB sensors for the ranging error is not considered in any of the research mentioned above. Though differences in the errors based on orientation between the ranging sensors were observed [28], it was still ignored for the calibration. In the proposed distance-bias calibration this orientation effect is considered by introducing the UWB center point vector, $\overrightarrow{C_s}$ in the calibration model. The effect of neglecting the effect of relative orientation of both UWB sensors in a ranging operation was verified by the higher errors in the uncalibrated distance measures compared against the measured casing origin point vector when compared to the errors validated against the distances with the $\overrightarrow{C_s}$ considered. Also, when the UWB modules used are bigger, then the errors will be bigger when the orientation effect is ignored. Therefore, the orientation effect has a significant contribution, and the proposed distance-bias method does compensate for this effectively.

The calibration algorithm in this article is only proposed for a swarm of three sensors, however, this could be further expanded based on the same equations and methods proposed. Expanding the equations for more sensors however increases the computation cost of the optimization, especially since an increase in each sensor node will lead to n-1 additive factorial number of equations (Equation (8). Thus, a practical approach would be to split the total sensor set available into sets of 3 for optimization. Whether repeating this process in other permutations of the sensor groupings and averaging results (like was done in this study for practical reasons) would improve overall calibration accuracy is subject to further studies. The same applies to investigating whether expanding the equation and performing optimization for larger sensor sets is possibly improving accuracy. Also, although attempts were made, the experiments in this study could possibly contain data samples from NLOS situations, which are expected to deteriorate the quality of the calibration outcome. Possibly the calibration procedure could be improved by avoiding NLOS situations 100 % by design or by detection and removal of values from the calibration recordings that are affected by NLOS errors.

Proposed distance-bias calibration is considered to be a one-time calibration to be performed in clear LOS with no external interference, after performing the antenna calibration recommended by the manufacturer and before first use. However, the validity of the calibration over time is yet to be tested. Also, in terms of the infrastructure required for generating reference data for this calibration procedure complex systems such as the optical motion capture system could possibly be substituted with MIMU-based, or preferably UMIMU-based, reference data generating methods. Also, the manual performance of the calibration protocol movements could be possibly replaced by movements performed by a robotic system, especially in an in-factory calibration procedure.

The distance-bias calibration method appeared to be capable of consistently removing a large part of the observable systematic errors in the distance estimates. This supports the validity of the main underlying assumption that these errors can be attributed to individual sensors as additive errors, within the tested distance range, relevant for application in only on-body applications for 3D analysis of human movement. A practical consequence of the fact that the proposed distance-bias calibration method only acts on the observed distance estimates and sensor orientations is, that it can be applied to data acquired with any similar UWB ranging system without access to internal UWB sensor hard- or software settings. The distance-bias calibration deals only with the systematic errors and the UWB sensors could provide accurate distance estimates with a very low residual systematic error in clear LOS situations. However, additional errors due to the external interferences and NLOS are expected in the intended application scenario. Therefore, these errors due to the external interferences and NLOS situations should be further studied for the successful application in human movement analysis. It is expected that the improved accuracy in UWB distance estimation within the relevant distance range under LOS conditions facilitates future development of improved 3D position estimation through smart data fusion algorithms applied to data from a swarm of integrated UWB and MIMU sensors on the human body (UMIMU sensor system) in the intended application of ambulatory 3D analysis of human movement.

5. Conclusion

In this article, a novel distance-bias calibration algorithm was proposed for minimizing the apparent systematic UWB sensor distance estimate errors, assuming these are attributable to fixed contributions of individual UWB sensors in a swarm network. This is done by exploiting the redundancy in the distance estimates in a fully connected sensor swarm. The performance of the distance-bias calibration algorithm is validated with a synthetic data set and with an experimental data set on multiple swarms of 3 sensors. The validation with synthetic data confirmed the calibration algorithm's capability to reliably converge and estimate the systematic error parameters attributed to the different sensors with high and consistent accuracy. The validation with experimental data within a distance range relevant for future application in the 3D analysis of human movement further confirmed that the calibration protocol can reduce the systematic error component consistently to below or equal to 0.5 cm in magnitude, which is more accurate than any other methods reported in the literature. It was also shown that at these accuracy levels, it is also essential to represent the UWB sensor module position not by a reference point on the sensor casing, but by the actual effective positions within the casing of the 2 sensors that the UWB ranging hardware uses for distance estimation. This requires simultaneous observation during the calibration measurements of both the sensor casing positions (by the reference system) and their 3D orientations (by the MIMUs or the reference system). As a byproduct, the calibration procedure also delivers these effective positions with respect to the sensor casing reference frames consistently within the antenna surface of UWB nodes. The accuracy levels achieved with the proposed method promise to facilitate future development of improved 3D position estimation methods through a smart data fusion approach applied to a swarm of integrated UWB/MIMU sensors (UMIMU sensor swarm) with an accuracy required for clinically relevant application in ambulatory 3D analysis of human movement.

CRediT authorship contribution statement

Vinish Yogesh: Writing – original draft, Validation, Methodology, Formal analysis, Conceptualization. **Lisanne Grevinga:** Validation, Methodology, Formal analysis. **Carsten Voort:** Methodology. **Jaap H.**

Buurke: Writing – review & editing, Supervision. **Peter H. Veltink:** Writing – review & editing, Supervision. **Chris T.M. Baten:** Writing – review & editing, Supervision, Project administration, Funding acquisition, Conceptualization.

Declaration of Competing Interest

The authors declare that they have no known competing financial interests or personal relationships that could have appeared to influence the work reported in this paper.

Funding

This research was funded by the European Fund for Regional Development (EFRO) under grant number PROJ-000965.

References

[1] Filippeschi, A.; Schmitz, N.; Miezal, M.; Bleser, G.; Ruffaldi, E.; Stricker, D. Survey of Motion Tracking Methods Based on Inertial Sensors: A Focus on Upper Limb Human Motion. Sensors (Basel) 2017, 17, doi:10.3390/s17061257.

[2] A.M. Sabatini, Estimating Three-Dimensional Orientation of Human Body Parts by Inertial/Magnetic Sensing, Sensors (basel) 11 (2011) 1489–1525, https://doi.org/10.3390/s110201489.

[3] D. Roetenberg, H.J. Luinge, C.T. Baten, P.H. Veltink, Compensation of Magnetic Disturbances Improves Inertial and Magnetic Sensing of Human Body Segment Orientation, IEEE Transactions on Neural Systems and Rehabilitation Engineering 13 (2005) 395–405, https://doi.org/10.1109/TNSRE.2005.847353.

[4] Schön, T.B.; Hol, J.D.; Kok, M. Using Inertial Sensors for Position and Orientation Estimation. Foundations and Trends® in Signal Processing 2017, 11, 1-153, doi:10.1561/2000000094.

[5] R.V. Vitali, R.S. McGinnis, N.C. Perkins, Robust Error-State Kalman Filter for Estimating IMU Orientation, IEEE Sensors Journal 21 (2021) 3561–3569, https://doi.org/10.1109/jsen.2020.3026895.

[6] Chow, J.; Hol, J.; Luinge, H. Tightly-Coupled Joint User Self-Calibration of Accelerometers, Gyroscopes, and Magnetometers. Drones 2018, 2, doi:10.3390/drones2010006.

[7] Kaichi, T.; Maruyama, T.; Tada, M.; Saito, H. Resolving Position Ambiguity of IMU-Based Human Pose with a Single RGB Camera. Sensors (Basel) 2020, 20, doi:10.3390/s20195453.

[8] H.J. Luinge, P.H. Veltink, C.T. Baten, Ambulatory Measurement of Arm Orientation, Journal of Biomechanics 40 (2007) 78–85, https://doi.org/10.1016/j.jbiomech.2005.11.011.

[9] Ma, M.; Song, Q.; Gu, Y.; Li, Y.; Zhou, Z. An Adaptive Zero Velocity Detection Algorithm Based on Multi-Sensor Fusion for a Pedestrian Navigation System. Sensors (Basel) 2018, 18, doi:10.3390/s18103261.

[10] J. Wahlstrom, I. Skog, Fifteen Years of Progress at Zero Velocity: A Review, IEEE Sensors Journal 21 (2021) 1139–1151, https://doi.org/10.1109/jsen.2020.3018880.

[11] D. Weenk, D. Roetenberg, B.J. van Beijnum, H.J. Hermens, P.H. Veltink, Ambulatory Estimation of Relative Foot Positions by Fusing Ultrasound and Inertial Sensor Data, IEEE Transactions on Neural Systems and Rehabilitation Engineering 23 (2015) 817–826, https://doi.org/10.1109/TNSRE.2014.2357686.

[12] T.N. Hung, Y.S. Suh, Inertial Sensor-Based Two Feet Motion Tracking for Gait Analysis, Sensors (basel) 13 (2013) 5614–5629, https://doi.org/10.3390/s130505614.

[13] R.F. Brena, J.P. García-Vázquez, C.E. Galván-Tejada, D. Muñoz-Rodriguez, C. Vargas-Rosales, J. Fangmeyer, Evolution of Indoor Positioning Technologies: A Survey, Journal of Sensors 2017 (2017) 1–21, https://doi.org/10.1155/2017/2630413.

[14] Hayward, S.J.; van Lopik, K.; Hinde, C.; West, A.A. A Survey of Indoor Location Technologies, Techniques and Applications in Industry. Internet of Things 2022, 20, doi:10.1016/j.iot.2022.100608.

[15] A. Poulose, O.S. Eyobu, D.S. Han, An Indoor Position-Estimation Algorithm Using Smartphone IMU Sensor Data, IEEE Access 7 (2019) 11165–11177, https://doi.org/10.1109/access.2019.2891942.

[16] Yao, L.; Yao, L.; Wu, Y.W. Analysis and Improvement of Indoor Positioning Accuracy for UWB Sensors. Sensors 2021, 21, doi:10.3390/s21175731.

[17] X.F. Yang, J. Wang, D.P. Song, B.Z. Feng, H. Ye, A Novel NLOS Error Compensation Method Based IMU for UWB Indoor Positioning System, IEEE Sensors Journal 21 (2021) 11203–11212, https://doi.org/10.1109/JSEN.2021.3061468.

[18] R.K. Yadav, B. Bhattarai, H.S. Gang, J.Y. Pyun, Trusted K Nearest Bayesian Estimation for Indoor Positioning System, IEEE Access 7 (2019) 51484–51498, https://doi.org/10.1109/ACCESS.2019.2910314.

[19] A. Buffi, A. Michel, P. Nepa, B. Tellini, RSSI Measurements for RFID Tag Classification in Smart Storage Systems, IEEE Transactions on Instrumentation and Measurement 67 (2018) 894–904, https://doi.org/10.1109/tim.2018.2791238.

[20] Minne, K.; Macoir, N.; Rossey, J.; Brande, Q.V.D.; Lemey, S.; Hoebeke, J.; Poorter, E. Experimental Evaluation of UWB Indoor Positioning for Indoor Track Cycling. Sensors (Basel) 2019, 19, doi:10.3390/s19092041.

[21] F. Mazhar, M.G. Khan, B. Sällberg, Precise Indoor Positioning Using UWB: A Review of Methods, Algorithms and Implementations, Wireless Personal Communications 97 (2017) 4467–4491, https://doi.org/10.1007/s11277-017-4734-x.

[22] X. Li, Y. Wang, D. Liu, Research on Extended Kalman Filter and Particle Filter Combinational Algorithm in UWB and Foot-Mounted IMU Fusion Positioning, Mobile Information Systems 2018 (2018), https://doi.org/10.1155/2018/1587253.

[23] Yogesh, V.; Buurke, J.H.; Veltink, P.H.; Baten, C.T.M. Integrated UWB/MIMU Sensor System for Position Estimation towards an Accurate Analysis of Human Movement: A Technical Review. Sensors 2023, 23, doi:10.3390/s23167277.

[24] G. Yavuzer, O. Oken, A. Elhan, H.J. Stam, Repeatability of Lower Limb Three-Dimensional Kinematics in Patients with Stroke, Gait & Posture 27 (2008) 31–35, https://doi.org/10.1016/j.gaitpost.2006.12.016.

[25] M. Windolf, N. Gotzen, M. Morlock, Systematic Accuracy and Precision Analysis of Video Motion Capturing Systems-Exemplified on the Vicon-460 System, Journal of Biomechanics 41 (2008) 2776–2780, https://doi.org/10.1016/j.jbiomech.2008.06.024.

[26] B. Carse, B. Meadows, R. Bowers, P. Rowe, Affordable Clinical Gait Analysis: An Assessment of the Marker Tracking Accuracy of a New Low-Cost Optical 3D Motion Analysis System, Physiotherapy 99 (2013) 347–351, https://doi.org/10.1016/j.physio.2013.03.001.

[27] E. van der Kruk, M.M. Reijne, Accuracy of Human Motion Capture Systems for Sport Applications; State-of-the-Art Review, European Journal of Sport Science 18 (2018) 806–819, https://doi.org/10.1080/17461391.2018.1463397.

[28] De Preter, A.; Goysens, G.; Anthonis, J.; Swevers, J.; Pipeleers, G. Range Bias Modeling and Autocalibration of an UWB Positioning System. In Proceedings of the 2019 International Conference on Indoor Positioning and Indoor Navigation (IPIN), Pisa, Italy, 2019; pp. 1-8.

[29] Shalaby, M.A.; Cossette, C.C.; Forbes, J.R.; Ny, J.L. Calibration and Uncertainty Characterization for Ultra-Wideband Two-Way-Ranging Measurements. In Proceedings of the 2023 IEEE International Conference on Robotics and Automation (ICRA), London, United Kingdom, 2023; pp. 4128-4134.

[30] S. Shah, K. Chaiwong, L.-O. Kovavisaruch, K. Kaemarungsi, T. Demeechai, Antenna Delay Calibration of UWB Nodes, IEEE Access 9 (2021) 63294–63305, https://doi.org/10.1109/access.2021.3075448.

[31] J. Cano, G. Pages, E. Chaumette, J. LeNy, Clock and Power-Induced Bias Correction for UWB Time-of-Flight Measurements, IEEE Robotics and Automation Letters 7 (2022) 2431–2438, https://doi.org/10.1109/lra.2022.3143202.

[32] APS014 Application Note, Antenna Delay Calibration of DW1000-Based Products and Systems. Available online: https://www.qorvo.com/products/d/da008449 (accessed on June 25, 2023).

[33] Sidorenko, J.; Schatz, V.; Scherer-Negenborn, N.; Arens, M.; Hugentobler, U. Decawave UWB Clock Drift Correction and Power Self-Calibration. Sensors (Basel) 2019, 19, doi:10.3390/s19132942.

[34] B. Alavi, K. Pahlavan, Modeling of the TOA-based distance measurement error using UWB indoor radio measurements, IEEE Communications Letters 10 (2006) 275–277, https://doi.org/10.1109/LCOMM.2006.1613745.

[35] Neirynck, D.; Luk, E.; McLaughlin, M. An Alternative Double-Sided Two-Way Ranging Method. In Proceedings of the 2016 13th workshop on positioning, navigation and communications (WPNC), 2016; pp. 1-4.

[36] Lian Sang, C.; Adams, M.; Hormann, T.; Hesse, M.; Porrmann, M.; Ruckert, U. Numerical and Experimental Evaluation of Error Estimation for Two-Way Ranging Methods. Sensors (Basel) 2019, 19, doi:10.3390/s19030616.